A CANDIDATE $Z \sim 10$ GALAXY ARCED BY LENSING

Brett Salmon[1,†], Dan Coe[1], Larry Bradley[1], Marusa Bradač[2], Kuang-Han Huang[2], Pascal Oesch[3], Gabriel B. Brammer[1], Daniel Stark[4], Keren Sharon[5], Michele Trenti[6], Roberto J. Avila[1], Sara Ogaz[1], Ana Acebron[7], Felipe Andrade-Santos[8], Daniela Carrasco[6], Catherine Cerny[5], Nathália Cibirka[7], William Dawson[9], Brenda L. Frye[4], Austin Hoag[2], Christine Jones[8], Ramesh Mainali[5], Masami Ouchi[10,11], Rachel Paterno-Mahler[5], Avery Peterson[5], Steven A. Rodney[12], Keiichi Umetsu[13], Adi Zitrin[7]

[1]Space Telescope Science Institute, Baltimore, MD, USA,
[2]Department of Physics, University of California, Davis, CA 95616, USA,
[3]Geneva Observatory, University of Geneva, Ch. des Maillettes 51, 1290 Versoix, Switzerland,
[4]Department of Astronomy, Steward Observatory, University of Arizona, 933 North Cherry Avenue, Rm N204, Tucson, AZ, 85721, USA,
[5]Department of Astronomy, University of Michigan, 1085 South University Ave, Ann Arbor, MI 48109, USA,
[6]School of Physics, University of Melbourne, VIC 3010, Australia,
[7]Physics Department, Ben-Gurion University of the Negev, P.O. Box 653, Beer-Sheva 84105, Israel
[8]Harvard-Smithsonian Center for Astrophysics, 60 Garden Street, Cambridge, MA 02138, USA,
[9]Lawrence Livermore National Laboratory, P.O. Box 808 L- 210, Livermore, CA, 94551, USA,
[10]Institute for Cosmic Ray Research, The University of Tokyo, 5-1-5 Kashiwanoha, Kashiwa, Chiba 277-8582, Japan
[11]Kavli Institute for the Physics and Mathematics of the Universe (Kavli IPMU, WPI), The University of Tokyo, 5-1-5 Kashiwanoha, Kashiwa, Chiba, 277-8583, Japan
[12]Department of Physics and Astronomy, University of South Carolina, 712 Main St., Columbia, SC 29208, USA,
[13]Institute of Astronomy and Astrophysics, Academia Sinica, PO Box 23-141, Taipei 10617, Taiwan
Draft version December 4, 2017

ABSTRACT

Candidate galaxies at $z > 9$ are precious because they are seen in far fewer numbers than expected from existing luminosity functions, implying that the early universe underwent an era of rapid galaxy evolution. We present here the discovery of a particularly fortuitous $z = 10.0$ galaxy candidate which has been arced by the effects of strong gravitational lensing. Found in the large *Hubble Space Telescope* Reionization Lensing Cluster Survey (RELICS) and companion S-RELICS *Spitzer* program, this candidate has a lensed H-band magnitude of 25.8 AB mag. Depending on the uncertainty in the lensing magnification ($\mu \approx 4 - 7$) this corresponds to a de-lensed magnitude of $27.9-27.3$ AB mag, which is consistent with the observed magnitudes of other $z > 9$ candidates. The inferred upper limits on the stellar mass ($\log[M_\star/M_\odot] = 9.5^{+0.3}_{-0.3}$) and star formation rate ($\log[\text{SFR}/M_\odot \text{ yr}^{-1}] = 1.5^{+0.2}_{-0.2}$) indicate that this candidate is a typical star-forming galaxy on the $z > 6$ SFR–$M_\star$ relation. On the other hand, we rule out the only low-z solution as unphysical based on the required stellar mass, dust attenuation, size, and [OIII] EW needed for a $z \sim 2$ SED to match the data. Finally, we reconstruct the source-plane image and estimate the candidate's physical size at $z \sim 10$, finding a half-light radius of $r_e < 0.8$ kpc that is in line with the sizes of other $z > 9$ candidates. While the *James Webb Space Telescope* will detect $z > 10$ with ease, this rare candidate offers the potential for unprecedented spatial resolution less than 500 Myr after the Big Bang.

1. INTRODUCTION

With its high resolution and sensitivity, observations using the *Hubble Space Telscope* (*HST*) have accelerated our understanding of the high-z universe. Deep and wide extragalactic imaging surveys with ACS and WFC3 have uncovered thousands of galaxies at $z > 6$ in blank fields (see Finkelstein 2016; Stark 2016, for reviews), including the most distant galaxy found to-date (Oesch et al. 2016, GN-z11;). In addition, we have prioritized *HST* to observe the most massive galaxy clusters, taking advantage of the natural telescopes they create via strong gravitational lensing (CLASH; PI Postman, Frontier Fields; PI Lotz, RELICS; PI Coe). This investment in lensing fields in particular has proven fruitful. We have discovered highly magnified (MACS1149-JD, Zheng et al. 2012; Hoag et al. 2017; M0416-JDl, Infante et al. 2015) and multiply-imaged galaxies (MACS0647-JD, Coe et al. 2013; A2744-JD, Zitrin et al. 2014) at redshifts up to $z = 11$, which have allowed us to study faint UV metal

† bsalmon@stsci.edu

lines (Rigby et al. 2015; Stark et al. 2014; Mainali et al. 2017), nebular emission lines (Huang et al. 2016; Rydberg et al. 2017; Hoag et al. 2017), and the star formation rate density deep into the epoch of reionization (Oesch et al. 2012, 2014, 2017; Bouwens et al. 2014).

However, little is known in detail about the $z > 9$ universe, and the handful of candidates found so far exhibit peculiar properties. MACS0647-JD has a radius smaller than 100 pc, the size of Giant Molecular Clouds in the local universe. GN-z11 is three times brighter than the characteristic UV luminosity (L_*) of galaxies at that distance, surprisingly bright given the CANDELS search area. Both z~10 candidates MACS1149-JD and M0416-JD appear to have an evolved stellar population of ≈ 340 Myr, when the age of the universe was only ≈ 500 Myr (Hoag et al. 2017). *JWST* NIRCam will better sample the rest-frame UV-to-optical colors which will allow us to break some parameter degeneracies and challenge these initial inferences. However, with typical $z \sim 10$ effective radii of $< 0.2''$ and a NIRCAM PSF of $\sim 0.1''$, we will still be unable resolve these galaxies physically. Ideally, we would use the help of strong grav-

itational lensing to study the kinematics and intrinsic stellar populations at $z \sim 10$ in detail.

In this Letter we present a galaxy gravitationally lensed into an arc with a photo-z of $z_{\rm phot} = 10.0$, which we name SPT0615-JD ("JD" for *HST* F125W *J*-band dropout). Found behind the Reionization Lensing Cluster Survey (RELICS) cluster SPT0615-57, the arced features of SPT0615-JD extend across $\sim 2.5''$, allowing unprecedented physical resolution deep in the epoch of reionization. SPT0615-JD has an 11-σ detection in the *HST* F160W *H*-band and an AB magnitude of 25.7 AB, making it bright enough for follow-up spectroscopic or grism observations. In this work, we will present the supporting evidence that this candidate is indeed at $z \sim 10$, and discuss the remaining uncertainties.

2. DATA

The cluster SPT-CL J0615-5746 was originally targeted by the South Pole Telescope survey and found to be a promising strong gravitational lensing field given the relatively high cluster mass ($6.8 \times 10^{14}\ M_\odot$) for its high redshift, $z = 0.972$ (Williamson et al. 2011; Bleem et al. 2015). It was later followed up with *HST* as one of the RELICS cluster fields (see overview by Coe et al. in prep.). RELICS reached 5-σ limiting depths with ACS/WFC of 27.2, 27.6, and 27.1 AB magnitudes in respectively in F435W, F606W, and F814W (B, V, and I bands), and WFC3/IR depths of 26.6, 26.0, 26.2, and 26.5 respectively in F105W, F125W, F140W, and F160W (Y, J, JH, and H bands). The details of the SExtractor (version 2.8.6; Bertin & Arnouts 1996) object selection and *HST* photometry are described by Salmon et al. (2017) and Coe et al. (in prep). SPT0615-57 was the second highest high-z-producing cluster fields out of the 41 RELICS fields, revealing 25 new candidate galaxies over the redshift range $5.5 < z < 8.5$ (Salmon et al. 2017). It is sensible that this field may also contain the most distant candidate found by the program, given the aptitude of this field to produce many high-z candidates, due to the distant position of the massive cluster lens.

Fig. 1 shows image cutouts of the $z \sim 10$ candidate SPT0615-JD in each of the available *HST* bands, as well as a color composite. The bands blueward of F140W are undetected with S/N$\lesssim$2, and the F140W S/N is also very low (S/N$\sim$3). The galaxy is bright in F160W with S/N$\sim$11, showing an extended arc shape consistent with the direction of lensing shear expected from the cluster. Importantly, we emphasize that observed-frame size of SPT0516-JD is rather large ($\sim 2''$ in the tangential direction), which offers promising spatial resolution for *JWST* (see § 6).

The *Spitzer*-RELICS programs (PI Bradač, PI Soifer) provide flux from IRAC channel 1 and 2 bands at 3.6 μm and 4.5 μmwith $\approx$5-hour depth per band. These bands correspond to rest-frame optical flux at $z \sim 9$-10 and are invaluable for distinguishing between $z \sim 10$ star-forming galaxies and $z \sim 2$-3 interloper galaxies. A combination of strong emission lines and a dusty spectral energy distribution (SED) at $z \sim 2$-3 can reproduce the sharp break in *HST* colors, making it difficult to claim a very high-redshift solution (Vulcani et al. 2017). The low observed *Spitzer* fluxes

<< include TPHOT photometry details here >>.

In Fig. 1 we see image cutouts of the *Spitzer* 3.5μm
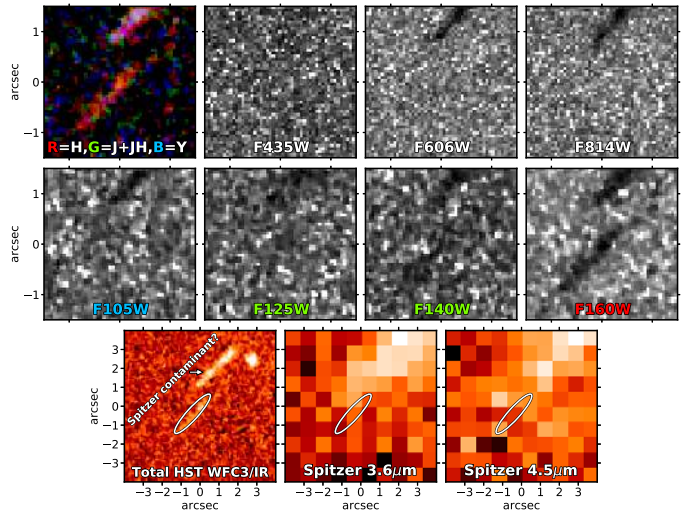
FIG. 1.— Individual-band images of SPT0615-JD (60 mas resolution). The top left panel is an RGB image with the R channel as F160W, the G channel as the sum of F125W and F140W, and the B channel as F105W. The remaining top panels are ACS images, followed by WFC3/IR images in the bottom row, all $3''$x$3''$. The candidate is missing in the bands blueward of F140W, indicating some strong spectral break. Bottom left: A weighted stack of all 4 WFC3/IR bands, centered on an $8''$x$8''$cutout of SPT0615-JD. Bottom middle, right: Cutouts of the *Spitzer* 3.6 μm and 4.5 μm images. Ellipses mark the position of SPT0615-JD. The nearby $z \sim 3$ galaxy likely contaminates the fluxes of the $z \sim 10$ candidate, even after attempts to subtract the neighboring flux.

and 4.5μm images centered on SPT0615-JD. Due to the neighboring, bright $z \sim 3$ galaxy, the observed *Spitzer* fluxes are highly uncertain, and should be considered as upper limits. Even so, the observed fluxes in each *Spitzer* band are already several orders of magnitude less faint than typical low-z interlopers. This is critical because while all $z \sim 10$ solutions could have lower *Spitzer* fluxes, the $z \sim 2$ solution *requires* them to be high. As we will discuss in § 3, the inflated *Spitzer* fluxes also increase the inferred $z \sim$10 UV dust attenuation, which should also be considered as an upper limit. We have already proposed for deeper *Spitzer* observations and received director discretionary time to observe this and other RELICS clusters.

3. SED FITTING

Thanks to the *Spitzer* data that probes the rest-frame optical, we can infer upper-limits on physical parameters like stellar mass and dust attenuation to test if the high or low-redshift solutions are sensible. We use a Bayesian SED-fitting procedure originally described by Papovich et al. (2001, 2006) and updated by Salmon et al. (2015). In short, we sample the posterior using a grid of SEDs that represent a range of stellar population ages (10 Myr $< t_{\rm age} < t_{\rm universe}$, logarithmically spaced), attenuation ($0 < A_{\rm UV} < 7.4$), metallicity ($2\% Z_\odot < Z < Z_\odot$), and rising star-formation histories ($\Psi(t) = \Psi_0 \exp(t/\tau_{\rm SFH})$, where the e-folding timescale $\tau_{\rm SFH}$ can be 0.3, 0.5, 0.7, 1, 3, 5, 7, 10, 30, 50, 70, or 100 Gyr). We use Bruzual & Charlot (2003) stellar population synthesis models with a Chabrier (2003) IMF[2] and include the effects of nebular emission lines

---

[2] Switching from a Chabrier to a Salpeter (1955) IMF would require increasing the stellar mass and star-formation rate (SFR)
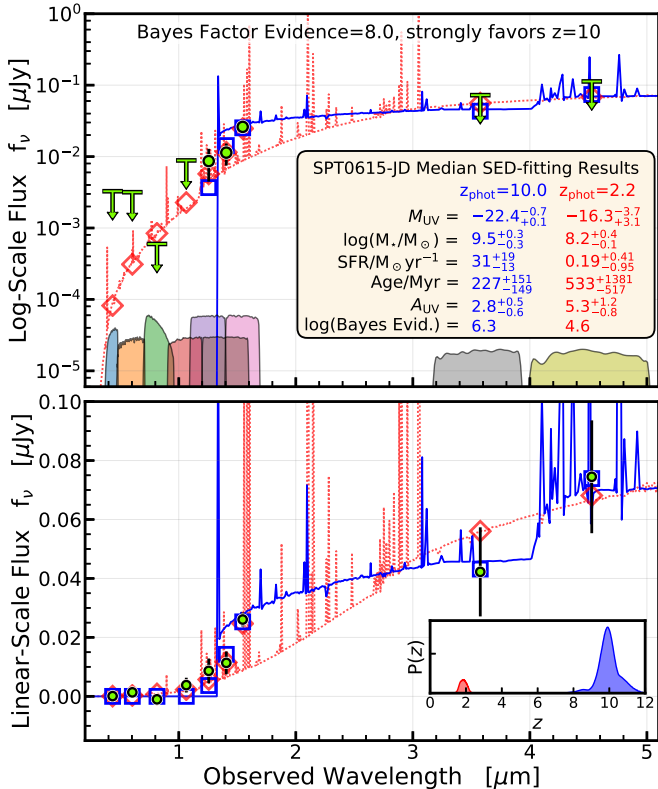
FIG. 2.— Best-fit SED to the RELICS data (green circles) of SPT0615-JD (solid blue line). The squares show the best-fit SED model fluxes. Including the relatively faint *Spitzer* fluxes (shown as triangles) the redshift likelihood P(z) strongly favors the $z = 10$ solution. The lower likelihood $z \sim 2$ solution is shown as the dotted red line. Even with the current data, this candidate has a strong $z = 10$ photo-z, with a $z < 3$ likelihood of only $\approx 10\%$.

following Salmon et al. (2015). We assume the dust-attenuation law derived by Salmon et al. (2016) that varies in shape from a steep law at low at low attenuation (similar in shape to the extinction law of the Small Magellanic Cloud) to a grey law at high attenuation (similar in shape to the starburst curve of Calzetti et al. (2000)).

The results of our SED fitting are summarized in Fig. 2. The fits assuming the $z \sim 10$ redshift show a moderately high stellar mass of $M_\star = 10^{9.5}$ $M_\odot$ and star-formation rate of SFR=31 $M_\odot$/yr. However, the stellar mass, star-formation rate, age, and UV dust attenuation should all be lower if the rest-frame optical fluxes are over-estimated, as implied by the *Spitzer* contaminant shown in Fig. 1. Therefore, we consider these preliminary estimates to be upper limits. Nevertheless, the stellar mass and SFR of SPT0615-57 are indicative of a typical star-forming at $z \sim 10$ (Oesch et al. 2014) and would lie on the relation between SFR and stellar mass at $z \sim 6$ (Salmon et al. 2015).

The SED fit assuming $z \sim 2$ is quite different. The median, marginalized results, which account for the full probability density, imply a low stellar mass $M_\star = 10^{8.2}$ $M_\odot$, low star-formation rate SFR= $10^{-0.7}$ $M_\odot$/yr, and evolved stellar population age t=533 Myr, with high uncertainty. However, there is a small combination of parameters with higher likelihood that seem to match the data reasonably well. This best-

by 0.25 dex respectively.

fit SED has the same stellar mass, but a higher SFR (SFR= $10^{-0.7}$ $M_\odot$/yr), a very young age (t=10 Myr), very dusty SED ($A_{\rm UV} = 7.0$ mag), and extremely high nebular emission to match the F160W flux ([OIII]+H$_\beta$ equivalent width EW=1671 Å). This SED solution is unphysical for several reasons. Its dust attenuation is dramatically high for its low stellar mass (Pannella et al. 2009), its size is too large and SED too dusty compared to other extreme [OIII] emitting "green pea" galaxies at $z \sim 2$ (Cardamone et al. 2009; Malkan et al. 2017), and it has too high EW compared to [OIII] emitters at $z \sim 2$ of similar mass (Maseda et al. 2013; Khostovan et al. 2016). Finally, unlike the $z \sim 10$ solution, the $z \sim 2$ solution *requires* the already overestimated *Spitzer* fluxes to be high, and it becomes increasingly harder to justify a $z \sim 2$ SED with lower 3.5μm and 4.5μm flux.

We caution the reader that the best-fit, maximum-likelihood SEDs in Fig. 2 (and best-fit SED solutions in general) are not necessarily representative of the full probability density of the posterior (Leja et al. 2017). A better indicator of the goodness-of-fit than the best-fit χ^2 is the unconditional marginal likelihood of the data, or the Bayesian evidence (see e.g., Kauffmann et al. 2003; Salmon et al. 2016, for definitions), which describes probability of seeing the data given all parameters. The ratio of two Bayesian evidences[3] under different global model assumptions, such as whether we assume the SED lies at $z \sim 2$ or $z \sim$10, is called the Bayes Factor and is used to describe the relative evidence between the two model assumptions. We find a Bayes-Factor evidence of 8.0 in favor of the $z \sim 10$ solution, which is considered "strong" evidence (Kass & Raftery 1995). Our interpretation is that there are more SED scenarios that can reasonably match the data assuming the $z \sim 10$ redshift than the select few (and justifiably unphysical) SEDs that reasonably fit the data assuming the $z \sim 2$ redshift.

4. COUNTER IMAGES

Detecting counter images is important because we can compare their symmetry, deflection angle, and position to predict the relative lensing distance. Taking advantage of lower redshift galaxies with well-defined redshifts, we can therefore obtain geometric "proof" of the redshift, similar to the method by Zitrin et al. (2014) for A2744-JD at $z \sim 9.8$.

Our lens models predict two positions for counter-images that should be of similar brightness to SPT0615-JD. Fig. 3 shows the position of SPT0615-JD and the potential counter-image locations. One of the positions is at the HST/WFC3 detector edge and obscured by a bright foreground star. However, the second position should be in a relatively clear area but we do not as yet see a source with colors like a $z \sim 10$ candidate. However, the WFC3 imaging in this field is shallow and we cannot rule out that the counter image may be just fainter our detection limit. Follow-up imaging for this candidate, and the other 26 z=6–8 candidates in this field, is required

---

[3] Specifically, the Bayes-factor evidence is typically described as $\zeta = 2 \cdot \ln B_{12}$, where B_{12} is the ratio of the Bayesian evidence under model assumption 1 to that of model assumption 2. Kass & Raftery (1995) use this formalism to define descriptive statements of relative strength towards model 1 versus model 2, where larger positive numbers favor the assumptions in model 1, and negative favor the assumptions in model 2.

Salmon et al.
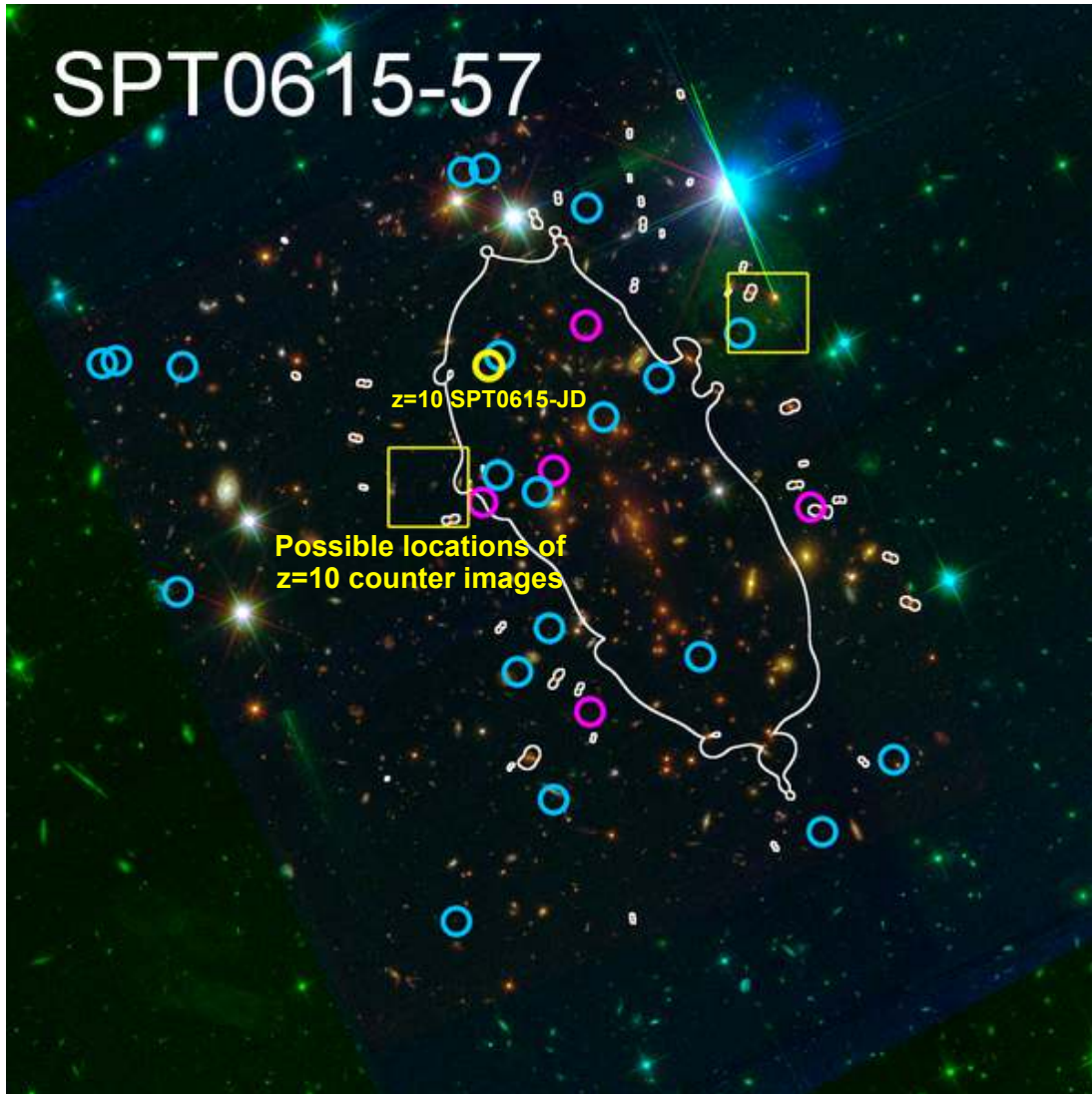
Fig. 3.— A $3\rlap{.}'25 \times 3\rlap{.}'25$ color image of the RELICS cluster SPT0615-57 marking the positions of all $z > 5.5$ candidates. The yellow circle marks the location of the $z = 10$ candidate SPT0615-JD. The yellow squares show the lens-model predictions for the locations of the counter images. The white lines represent the $z = 10$ critical curves of the lens model. The cyan and magenta circles mark the locations of the $z \sim 6$ and $z \sim 7 - 8$ candidate galaxies respectively.

to investigate this further.

5. MAG VS REDSHIFT

Finally, Fig. 4 shows the H-band magnitude as a function of redshift for all candidate galaxies in RELICS, compared to many other deep and wide surveys. SPT0615-JD stands out as an exceedingly rare high-z galaxy candidate, and its intrinsic de-lensed magnitude is similar to to that of the z=11 candidate MACS0647-JD. $<<$ More on this if we include image stamps of the other $z > 9$ canidates on this figure $>>$.

6. SIZES

An independent way to test if SPT0615-JD might actually be an interloper at lower redshift is to calculate its physical size and compare to other known interlopers. Moreover, the sizes of $z > 9$ galaxies can give us great physical insight into the initial conditions of early disk evolution. For example, analytical studies have formed a framework of galaxy size evolution based on the build-up of dark matter halo angular momentum and the accretion and cooling of baryons (Fall & Efstathiou 1980; Dalcanton et al. 1997; Mo et al. 1998), which was later refined by N-body (Navarro & Steinmetz 2000) and hydrodynamic simulations (Ma et al. 2017), and tested by empirical observations with HST (Ferguson et al. 2004; Bouwens et al. 2004, 2006, 2017; Oesch et al. 2010; Shibuya et al. 2015;
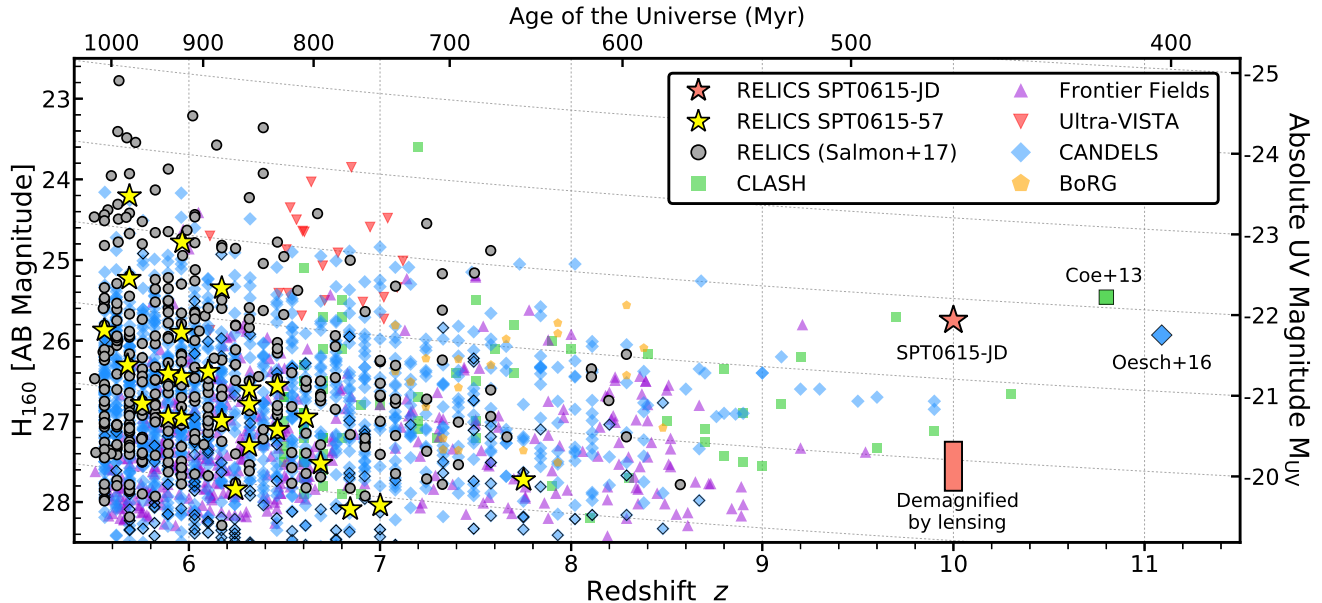
FIG. 4.— The H-band magnitude as a function of redshift. The high-z galaxy candidates from RELICS are shown as salmon-colored circles, with the light-salmon stars representing the other high-z candidates behind SPT0615-57. The $z = 10.0$ candidate SPT0615-JD is marked by the large yellow star. The yellow rectangle represents the range of de-magnified magnitudes of SPT0615-JD, according to the current range in magnification uncertainty, $\mu = 4 - 7$. Out of all of these excellent surveys, SPT0615-JD stands out both in redshift and magnitude, offering exquisite spatial resolution of an intrinsically faint galaxy less than 500 Myr after the Big Bang.

Curtis-Lake et al. 2016). Broadly, the $z > 5$ size evolution at fixed luminosity scales as $(1+z)^{-m}$ where m=1–2, giving us a baseline for physical sizes. In addition, Holwerda et al. (2015) demonstrated that a combination of UV-to-optical color, sampled by the F160W and 3.6 μm bands, and physical size can be used to identify obvious low-z contaminants. They summarized that the sizes of $z > 9$ galaxy candidates have typical half-light radii of $r_e < 0.8$ kpc.

To calculate the size of SPT0615-JD, we used out lens model to reconstruct its image in the source plane. The lens model finds a relatively mild tangential magnification, or shear, of a factor of ~ 3, leaving the full width of the source to be about 3–3.5 kpc. If we assume the light distribution is uniform, we can take take the half light radius to be about $\sim 1/4$ of the full size and find $r_e \approx 0.7$–0.8 kpc. The statistical error on this size (from the lens model) is only a couple of percent, so we are dominated by systematic errors ($\sim 10\%$). Curiously, the reconstructed source's axis ratio is still about 2:1 in the same direction as the lensing shear, which could mean that the shear is underestimated and the size is in fact smaller.

Fig. 5 shows that the inferred size of SPT0615-JD is typical compared to other high-z candidates. This pro-vides crucial evidence in support of the $z \sim 10$ solution that is independent of the galaxy SED. While the uncertainty in the $z \sim 10$ UV dust attenuation should be considered as an upper limit, the candidate is still within the range of $M_{\rm UV}$ and SFR surface density of known $z > 9$ candidates.

7. CONCLUSIONS

We present SPT0615-JD, a promising $z = 10.0$ galaxy candidate that appears to be arced by the effects of strong gravitational lensing. Out of all combined lensing fields from RELICS, CLASH, and the Frontier Fields, there is no other arced galaxy candidate as distant as SPT0615-JD. We find strong Bayesian evidence that the SED-inferred physical properties of this candidate are of a $z \sim 10$ typical star-forming galaxy. The only SED-fit that matches the $z \sim 2$ solution is unphysical based on the required combination of its size, mass, dust attenuation, and [OIII]+H$_\beta$ EW. Finally, the source-plane size of SPT0615-JD is typical of other star-forming galaxies, while the observed-frame offer unprecedented spatial resolution. This galaxy may be one of the most exciting targets for high-z science with $JWST$ as it offers the unique opportunity for resolving stellar populations deep in the epoch of reionization.

REFERENCES

Bertin, E., & Arnouts, S. 1996, A&AS, 117, 393
Bleem, L. E., Stalder, B., de Haan, T., et al. 2015, ApJS, 216, 27
Bouwens, R. J., Illingworth, G. D., Blakeslee, J. P., Broadhurst, T. J., & Franx, M. 2004, ApJ, 611, L1
Bouwens, R. J., Illingworth, G. D., Blakeslee, J. P., & Franx, M. 2006, ApJ, 653, 53
Bouwens, R. J., Illingworth, G. D., Oesch, P. A., et al. 2017, ApJ, 843, 41
Bouwens, R. J., Bradley, L., Zitrin, A., et al. 2014, ApJ, 795, 126
Bruzual, G., & Charlot, S. 2003, MNRAS, 344, 1000

Calzetti, D., Armus, L., Bohlin, R. C., et al. 2000, ApJ, 533, 682
Cardamone, C., Schawinski, K., Sarzi, M., et al. 2009, MNRAS, 399, 1191
Chabrier, G. 2003, PASP, 115, 763
Coe, D., Zitrin, A., Carrasco, M., et al. 2013, ApJ, 762, 32
Curtis-Lake, E., McLure, R. J., Dunlop, J. S., et al. 2016, MNRAS, 457, 440
Dalcanton, J. J., Spergel, D. N., & Summers, F. J. 1997, ApJ, 482, 659
Fall, S. M., & Efstathiou, G. 1980, MNRAS, 193, 189
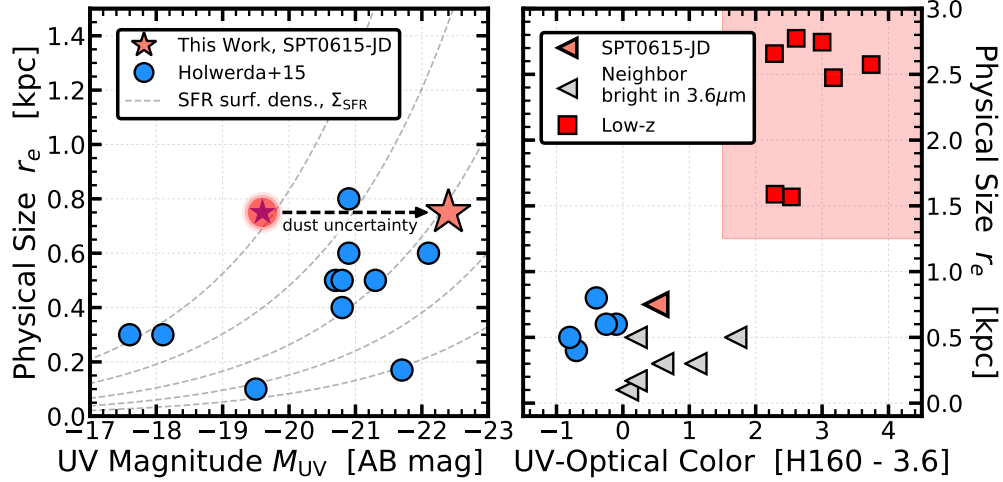
FIG. 5.— The physical size of SPT0615-JD compared to other known $z > 9$ galaxy candidates (blue circles). Left: the physical size as a function of UV magnitude. The upper-limit dust uncertainty is shown as the salmon-colored star, where the dust-obscured magnitude is shown as the red circle and star. Right: the physical size as a function of F160W-3.6μm color. Triangles show $z >$ candidates that may be contaminated in *Spitzer* flux by a bright neighbor, including SPT0615-JD (bold triangle). Typical sizes of very red low-z contaminants (red squares) are shown in the red box.

Ferguson, H. C., Dickinson, M., Giavalisco, M., et al. 2004, ApJ, 600, L107

Finkelstein, S. L. 2016, PASA, 33, e037

Hoag, A., Bradač, M., Trenti, M., et al. 2017, Nature Astronomy, 1, 0091

Holwerda, B. W., Bouwens, R., Oesch, P., et al. 2015, ApJ, 808, 6

Huang, K.-H., Lemaux, B. C., Schmidt, K. B., et al. 2016, ApJ, 823, L14

Infante, L., Zheng, W., Laporte, N., et al. 2015, ApJ, 815, 18

Kass, R. E., & Raftery, A. E. 1995, Journal of the American Statistical Association, 90, 773

Kauffmann, G., Heckman, T. M., White, S. D. M., et al. 2003, MNRAS, 341, 33

Khostovan, A. A., Sobral, D., Mobasher, B., et al. 2016, MNRAS, 463, 2363

Leja, J., Johnson, B. D., Conroy, C., van Dokkum, P. G., & Byler, N. 2017, ApJ, 837, 170

Ma, X., Hopkins, P. F., Boylan-Kolchin, M., et al. 2017, ArXiv e-prints, arXiv:1710.00008

Mainali, R., Kollmeier, J. A., Stark, D. P., et al. 2017, ApJ, 836, L14

Malkan, M. A., Cohen, D. P., Maruyama, M., et al. 2017, ApJ, 850, 5

Maseda, M. V., van der Wel, A., da Cunha, E., et al. 2013, ApJ, 778, L22

Mo, H. J., Mao, S., & White, S. D. M. 1998, MNRAS, 295, 319

Navarro, J. F., & Steinmetz, M. 2000, ApJ, 538, 477

Oesch, P. A., Bouwens, R. J., Illingworth, G. D., Labbe, I., & Stefanon, M. 2017, ArXiv e-prints, arXiv:1710.11131

Oesch, P. A., Bouwens, R. J., Illingworth, G. D., et al. 2010, ApJ, 709, L16

—. 2012, ApJ, 745, 110

—. 2014, ApJ, 786, 108

Oesch, P. A., Brammer, G., van Dokkum, P. G., et al. 2016, ApJ, 819, 129

Pannella, M., Carilli, C. L., Daddi, E., et al. 2009, ApJ, 698, L116

Papovich, C., Dickinson, M., & Ferguson, H. C. 2001, ApJ, 559, 620

Papovich, C., Moustakas, L. A., Dickinson, M., et al. 2006, ApJ, 640, 92

Rigby, J. R., Bayliss, M. B., Gladders, M. D., et al. 2015, ApJ, 814, L6

Rydberg, C.-E., Zitrin, A., Zackrisson, E., et al. 2017, MNRAS, 467, 768

Salmon, B., Papovich, C., Finkelstein, S. L., et al. 2015, ApJ, 799, 183

Salmon, B., Papovich, C., Long, J., et al. 2016, ApJ, 827, 20

Salmon, B., Coe, D., Bradley, L., et al. 2017, ArXiv e-prints, arXiv:1710.08930

Salpeter, E. E. 1955, ApJ, 121, 161

Shibuya, T., Ouchi, M., & Harikane, Y. 2015, ApJS, 219, 15

Stark, D. P. 2016, ARA&A, 54, 761

Stark, D. P., Richard, J., Siana, B., et al. 2014, MNRAS, 445, 3200

Vulcani, B., Trenti, M., Calvi, V., et al. 2017, ApJ, 836, 239

Williamson, R., Benson, B. A., High, F. W., et al. 2011, ApJ, 738, 139

Zheng, W., Postman, M., Zitrin, A., et al. 2012, Nature, 489, 406

Zitrin, A., Zheng, W., Broadhurst, T., et al. 2014, ApJ, 793, L12